24, 1508 (1996).

31 F. Pastorino, D. Stuart, M. Ponzoni, and T. M. Allen, *J. Controlled Rel.*, **74**, 69 (2001).

32 M. Mizu, T. Kimura, K. Koumoto, K. Sakurai, and S. Shinkai, *Chem. Commun.*, **2001**, 429.

33 In this paper, we use the code "AS-c-myb + s-SPG" to show a mixture of AS-c-myb and s-SPG. It does not always mean that the complex is formed in this mixture. When necessary, the complex is denoted by "AS-c-myb/s-SPG".

34 T. Gura, *Science*, **270**, 575 (1995).

35 I. Lebedeva and C. A. Stein, *Annu. Rev. Pharmacol. Toxicol.*, **41**, 403 (2001).

36 R. W. Wagner, *Nat. Medicine*, **1**, 1116 (1995).

37 R. W. Wagner, M. D. Matteucci, D. Grant, T. Hung, and B. C. Froehler, *Nat. Biotech.*, **14**, 840 (1996).

38 T. L. Burgess, E. F. Fisher, S. L. Ross, J. V. Bready, Y. X. Qian, L. A. Bayewitch, A. M. Cohen, C. J. Herrera, S. S. F. Hu, T. B. Kramer, F. D. Lott, F. H. Martin, G. F. Pierce, L. Simonet, and C. L. Farrell, *Proc. Natl. Acad. Sci. U.S.A.*, **92**, 4051 (1995).

39 L. A. Yakubov, E. A. Deeva, V. F. Zarytova, E. M. Ivanova, A. S. Ryte, L. V. Yurchenko, and V. V. Vlassov, *Proc. Natl. Acad. Sci. U.S.A.*, **86**, 6454 (1989).

40 C. Beltinger, H. U. Saragovi, R. M. Smith, L. LeSuter, N. Shah, L. DeDionisio, L. Christensen, A. Raible, L. Jarett, and A. M. Gewirtz, *J. Clin. Invest.*, **95**, 1814 (1995).

41 T. Matsumoto, M. Numata, T. Anada, M. Mizu, K. Koumoto, K. Sakurai, T. Nagasaki, and S. Shinkai, *Biochem. Biophys. Acta*, in press.

42 M. Fujimoto, A. Kuninaka, and H. Yoshino, *Agric. Biol. Chem.*, **38**, 777 (1974).

43 C. A. Stein, C. Subasinghe, K. Shinozuka, and J. S. Chen, *Nucleic Acids Res.*, **16**, 3209 (1988).

44 M. Mizu, K. Koumoto, T. Kimura, K. Sakurai, and S. Shinkai, *submitted to Biomaterials*.

45 A. G. Daniel and M. N. Leonard, *Antisense Res. Dev.*, **5**, 213 (1995).

46 C. A. Stein, J. L. Tonkinson, and L. Yakubov, *Pharmacol. Ther.*, **52**, 365 (1991).

47 W. Sanger, "Principles of Nucleic Acid Structure," Springer-Verlag, New York (1984).

48 J. Gunn, C. M. Holt, S. E. Francis, L. Shepherd, M. Grohmann, C. M. H. Newman, D. C. Crossman, and D. C. Cumberland, *Circ. Res.*, **80**, 520 (1997).

49 I. J. Moon, Y. Lee, C. S. Kwak, J. H. Lee, K. Chol, A. D. Schreiber, and J. G. Park, *Biochem. J.*, **346**, 295 (2000).

50 C. Melani, L. Rivoltini, G. Parmiani, B. Calabretta, and M. P. Colombo, *Cancer Res.*, **51**, 2897 (1991).

J|A|C|S
COMMUNICATIONS

Published on Web 06/18/2004

A Polysaccharide Carrier for Immunostimulatory CpG DNAs To Enhance Cytokine Secretion[‖]

Masami Mizu,[†] Kazuya Koumoto,[†] Takahisa Anada,[†] Takahiro Matsumoto,[‡] Munenori Numata,[‡] Seiji Shinkai,[‡] Takeshi Nagasaki,[§] and Kazuo Sakurai*,[†]

Department of Chemical Processes & Environments, The University of Kitakyushu, 1-1 Hibikino, Wakamatu-ku, Kitakyushu, Fukuoka 808-0135, Japan, Faculty of Engineering Department of Chemistry & Biochemistry, Graduate School of Engineering, Kyushu University, 6-10-1 Hakozaki, Higashi-ku, Fukuoka, Fukuoka 812-8581, Japan, and Department of Applied and Bioapplied Chemistry, Graduate School of Engineering, Osaka City University, 3-3-138 Sugimoto, Sumiyoshi-ku, Osaka 588-8585, Japan

Received December 27, 2003; E-mail: sakurai@env.kitakyu-u.ac.jp

Oligodeoxynucleotides containing unmethylated CpG sequences (CpG DNA) have been shown to stimulate a cell-mediated immune response for mammals.[1] This immune response is considered to be a defense system that mammals have evolved because unmethylated CpG sequence emerges more frequently in bacterial DNAs than in mammalian DNAs. Considerable attention is devoted to this response because CpG DNA can be extraordinarily effective adjuvants for many vaccines against infections agents, cancer antigens, and allergens.[1] Henmi et al.[2] demonstrated that CpG DNA can be recognized by Toll-like receptor 9 (TLR-9). The Toll-like receptor family is generally located on plasma membrane and can recognize bacterial cell wall components. However, Ahmad-Nejad et al.[3] demonstrated that TLR-9 is not localized on the cell surface, but intracellularily, predicting that if we can efficiently deliver CpG DNA to endosome and/or lysosome, the immune response can be enhanced and controlled artificially.

To deliver CpG DNA to intracellular endosome and/or lysosome, there are two major issues to overcome: instability of CpG DNA in biological fluids and low uptake efficiency into cells, similar issues for antisense DNA carriers.[5] Instability of CpG DNA is ascribed to hydrolysis mediated by deoxyribonuclease. The hydrolysis can be significantly suppressed by the use of phosphorothioates,[5] and thus many studies use phosphorothioate CpG DNAs. However, phosphorothioates can be bound to some plasma proteins in nonspecific manners, which can cause undesirable side effects. Therefore, CpG DNA carriers are required to prevent the phosphorothioates from forming such nonspecific interactions with proteins, as well as to protect them against hydrolysis mediated by deoxyribonuclease. Several materials have been studied as CpG DNA carriers. The liposomal delivery is one of the preferred methods;[6] however, there are some drawbacks in its use.[4]

Sakurai and Shinkai found that the β-(1 → 3)-D-glucan schizophyllan (SPG) forms a novel complex with some polynucleotides,[7] and the complex is applicable to an antisense DNA carrier.[8] Here, SPG is an extracellular polysaccharide produced by the fungus *Schizophyllan commune*, and the main chain consists of β-(1 → 3)-D-glucan and one β-(1 → 6)-D-glycosyl side chain linked to the main chain at every three glucose residues (Figure 1).[9] The complex is automatically dissociated when the pH becomes less than 6.0, because protonation of the nucleotide base induces conformational changes, which causes dissociation of the complex.[10] This pH response seems ideal for releasing the complexed CpG DNA in late endosome in which the pH is maintained about 5.0. The complexed oligonucleotides acquire stronger resistance to deoxyribonuclease-mediated hydrolysis and SPG can prevent the complexed phosphorothioate oligonucleotides from forming nonspecific interactions with plasma proteins.[11] These properties seem greatly advantageous as a CpG DNA carrier, and the main purpose of this communication is to present preliminary results to prove superiority of SPG for the carrier.

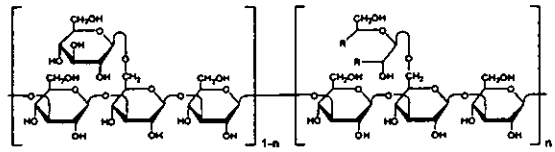

Figure 1. Chemical structure of the chemically modified schizophyllan (SPG) used in this study. The left-hand side shows the intact structure of SPG, and the right shows the modified one. The modification level in Table 1 is defined by "*n*" in the figure. The modification was made by the selective cleavage of 1,2-diol group of the glycosyl side chain with periodate, leading to formyl group formation and subsequently introducing a functional group (see Supporting Information).

Table 1. Sample Codes and the Introduced Chemical Groups

Sample code	R	Modification level[a]	N/P ratio[b]
SP-SPG	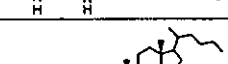	4.6 ± 0.3 mol%	0.27
Chol-SPG		6.9 ± 1.0 mol%	0.21
R8-SPG	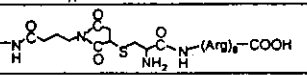	0.5 ± 0.1 mol%	~0
RGD-SPG	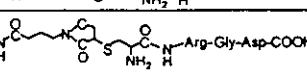	1.3 ± 0.3 mol%	~0

The uptake efficiency of SPG itself is not so high; therefore, we modified SPG with a functional group that can induce passive cellular ingestion. In this work, we introduced spermine (SP), arginine-glycine-aspartic acid tripeptide (RGD), octaarginine (R8), and cholesterol (Chol) (see Table 1). As CpG DNA, we used phosphorothioate 5′-TCCAT*GACGTT*CCTGATG-(dA)$_{40}$-3′ (the immunostimulatory sequence; PuPuCGPyPy is italicized).[12] For a negative control, we used the sequence of 5′-TCCATGA*GCTT*C-CTGAGT-(dA)$_{40}$-3′, where only the CG sequence is reversed (italic) and denoted "non-CpG DNA". In both sequences, a poly(dA)$_{40}$ tail is attached at the 3′ end to increase the complex stability.[7,8] The complexation was carried out by the established method,[7] and the molar ratio ($M_{s\text{-SPG}}/M_{ODN}$) was fixed to 1.5, where $M_{s\text{-SPG}}$ and M_{ODN} are the molar concentration of the repeating unit of SPG and

[‖] The 31st paper in the series Polysaccharide-Polynucleotide Complexes.
[†] University of Kitakyushu.
[‡] Kyushu University.
[§] Osaka City University.

10.1021/ja031978+ CCC: $27.50

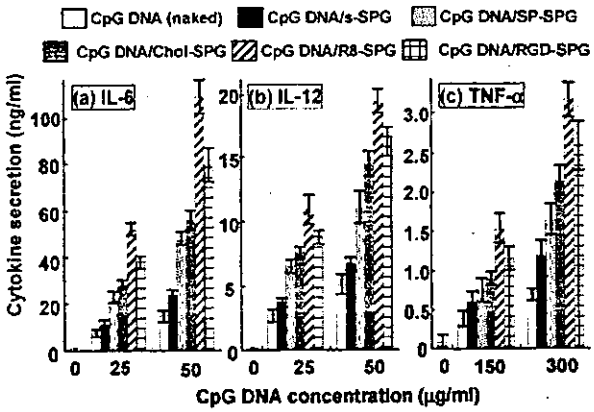

Figure 2. Effect of chemical modification of SPG on CpG DNA-mediated cytokine secretion. The murine macrophage-like cell J774.A1 (1×10^6 cells/mL, 100 μL/well) was stimulated with 25 and 50 μg/mL for IL-6 and IL-12 and with 150 and 300 μg/mL for TNF-α. The amount of secretions was determined with ELISA kits, after incubating the cells in the presence of CpG DNA or its complex for 24 h. The molar ratio ($M_{s\text{-SPG}}/M_{ODN}$) is fixed at 1.5.

CpG DNA, respectively. Although this molar ratio is in excess of SPG over the stoichiometric composition ($M_{s\text{-SPG}}/M_{ODN} = 2/3$),[7] the best antisense effect has been achieved at this composition.[8] Thus, we used this composition in the present work, and the total charge of the complex is maintained at negative at the composition.

When we exposed the murine macrophage-like cell J774.A1 to CpG DNA (complexed or naked), the cytokine secretion increased rapidly and reached a plateau after 9−15 h, being similar to the previous results.[12] After 24 h, all samples showed no increment and seemed to complete the secretion. Therefore, we evaluated the carrier performance from the amount of secreted cytokine after 24 h. Figure 2 plots the averaged amount of cytokine against the CpG DNA dose for three cytokines: IL-6 (a), IL-12 (b), and TNF-α (c), and the experimental variations are indicated by error bars.

When we exposed the cells to naked CpG DNA, the secretions of IL-6, IL-12, and TNF-α are 9.0 ± 1, 2.6 ± 1, and 0.75 ± 0.1 ng/mL, respectively. When the CpG DNA was added as a complex with nonmodified SPG (CpG DNA/s-SPG), the secretion is increased by about 20−40% from the naked assay. This difference should be ascribed to the facts that the complexed CpG DNA neither binds to serum proteins nor suffers hydrolysis from deoxyribonuclease,[11] although SPG itself does not have ability to enter cells. The modified SPG increases the secretion dramatically; it is 5−10-fold compared with the naked assays. Among them, R8−SPG shows the highest performance, RGD−SPG ranks the second, and Chol−SPG follows. The difference between RGD−SPG and Chol−SPG is prominent for IL-6; however, it is relatively small for IL-12 and TNF-α. As far as we know, this is the highest enhancement of the cytokine secretion by carriers.

The ingestion mechanism differs on introduced chemical moieties to the carrier. The cellular membrane is negatively charged, and therefore cations such as spermine can bind to the surface with the Coulombic forces and should be ingested by the regular pinocytosis cycle. This should be the case for SP−SPG; however, ingestion through the electrostatic interaction should not be effective for our case, because the complex is negatively charged in total (see Table 1). Therefore, it interferes with the spermine versus cell interaction. Generally, cholesterol-appended carriers are ingested through LDL receptor and RGD-appended ones, through integrins. Cellular ingestion for these is considered as receptor-mediated endocytosis. Therefore, after ingestion, the RGD−SPG or Chol−SPG/CpG DNA complex is eventually transported to endosome and finally to lysosome, where the compartment pH is kept to about 5 and digestive enzymes are highly activated. The complex releases the CpG DNA because of low pH,[10] and the naked CpG DNA is easily recognized by TLR-9 on the vesicular membrane. This may be a reason for the relatively high secretion for RGD−SPG and Chol−SPG complexes. In contrast with RGD, the arginine-rich peptides such as R8 are seemingly ingested by a different pathway from those of cations RGD and cholesterol, although there is still controversy and little agreement on the uptake mechanism.[13] Some data suggested that the pathway induced by R8 appears to deposit the R8-appended material directly into cytosol. If this were the only pathway to ingest the R8−SPG complex, the cytokine secretion would have been smaller than the others. The precise mechanism to uptake the R8−SPG complex and reason for such enhancement are not clear at this moment.

To sum up the present finding, when SPG is chemically modified with R8, RGD, and Chol and when the CpG DNA complex made therefrom is exposed to macrophages, dramatic enhancement in the cytokine secretion is observed. The secretion increased 5−10 times from the naked dose and 100 times from the background. This performance promises that SPG can be an excellent carrier for CpG DNA.

Acknowledgment. This work was financially supported by the JST SORST program.

Supporting Information Available: Experimental details, materials, SPG chemical modification procedures, cytotoxicity assay for the carriers, assay for non-CpG, confocal microscopy observation, and pH dependence of CD spectrum of the complex. This material is available free of charge via the Internet at http://pubs.acs.org.

References

(1) (a) Krieg A. M. *Biochim. Biophys. Acta* **1999**, *1489*, 107−116. (b) Krieg, A. M. *Nat. Med.* **2003**, *9*, 831−835.
(2) Hemmi, H.; Takeuchi, O.; Kawai, T.; Kaisho, T.; Sato, S.; Sanjo, H.; Matsumoto, M.; Hoshino, K.; Wagner, H.; Takeda, K.; Akira, S. *Nature* **2000**, *408*, 740−745.
(3) Ahmad-Nejad, P.; Häcker, H.; Rutz, M.; Bauer, S.; Vabulas, R. M.; Wagner, H. *Eur. J. Immunol.* **2002**, *32*, 1958−1968.
(4) Chirila, T. V.; Rakoczy, P. E.; Garrett, K. L.; Lou, X.; Constable, I. J. *Biomaterials* **2002**, *23*, 321−341.
(5) Stein, C. A.; Krieg, A. M. *Antisense Res. Dev.* **1994**, *4*, 67−69.
(6) (a) Gursel, I.; Gursel, M.; Ishii, K. J.; Klinman, D. *J. Immunol.* **2001**, *167*, 3324−3328. (b) Mui, B.; Raney, S. G.; Semple, S. C.; Hope, M. *J. Pharmacol. Exp. Ther.* **2001**, *298*, 1185−1192.
(7) (a) Sakurai, K.; Shinkai, S. *J. Am. Chem. Soc.* **2000**, *122*, 4520−4521 (b) Sakurai, K.; Shinkai, S.; Tabata, K. Japanese Patent 11-319470, 1999. (c) Sakurai, K.; Mizu, M.; Shinkai, S. *Biomacromolecules* **2001**, *2*, 641−650.
(8) Mizu, M.; Koumoto, K.; Anada, T.; Sakurai, K.; Shinkai, S. *Biomaterials* **2004**, *25*, 3109−3116
(9) Tabata, K.; Ito, W.; Kojima, T.; Kawabata, S.; Misaki, A. *Carbohydr. Res.* **1981**, *89*, 121−135.
(10) Sakurai, K.; Iguchi, R.; Mizu, M.; Koumoto, K.; Shinkai, S. *Bioorg. Chem.* **2003**, *31*, 216−226.
(11) Mizu, M.; Koumoto, K.; Kimura, T.; Anada, T.; Karinaga, R.; Nagasaki, T.; Sakurai, K.; Shinkai, S. *Bull. Chem. Soc. Jpn.* **2004**, *77*, 1101−1110.
(12) Aramaki, Y.; Yotsumoto, S.; Watanabe, H.; Tsuchiya, S. *Biol. Pharm. Bull.* **2002**, *25*, 351−355.
(13) (a) Futaki, S.; Nakase, I.; Suzuki, T.; Youjun, Z.; Sugiura, Y.; *Biochemistry* **2002**, *41*, 7925−7930. (b) Richard, J. P.; Melikov, K.; Vives, E.; Ramos C.; Verbeure, B.; Gait, M. J.; Chernomordik L. V.; Lebleu, B. *J. Biol. Chem.* **2003**, *278*, 585−590.

JA031978+

Separation Technique for Messenger RNAs by Use of Schizophyllan/Poly(A) Tail Complexation[1]

Taro Kimura,[†] Akiko Beppu,[†] Kazuo Sakurai,[‡] and Seiji Shinkai*[,§]

Fukuoka Industrial Technology Center, Biotechnology and Food Research Institute, 1465-5 Aikawa, Kurume 839-0861 Japan, Department of Chemical Processes and Environments, the University of Kitakyushu, 1-1 Hibikino Wakamatsu Kitakyushu 808-0135 Japan, and Department of Chemistry and Biochemistry, Graduate School of Engineering, Kyushu University, 6-10-1 Hakozaki, Fukuoka 812-8581 Japan

Received June 30, 2004; Revised Manuscript Received October 19, 2004

Schizophyllan (SPG) is one of the water soluble β-1,3-glucans and has a peculiar molecular recognition capability, namely, the single stranded SPG (s-SPG) can form a stoichiometric complex with certain polynucleotides such as poly(C) and poly(A), although it cannot bind poly(G) and poly(dC) at all. In this paper, we prepared an s-SPG-appended column and made an attempt to separate polynucleotides on the bases of this molecular recognition capability. The s-SPG-appended column trapped only such RNAs that could form the complex with s-SPG but eluted other RNAs which did not form the complex. Encouraged by the results in the model system, we extended the s-SPG-appended column into separation of native messenger RNAs (mRNAs) from a RNA mixture (total RNA) obtained from yeast. Since eukaryotic mRNAs have a poly(A) tail with 150−300 bases, we supposed that the tails would be trapped by the s-SPG-appended column. The results indicate that mRNAs were separated from total RNA in good yield and with high purity. It should be emphasized that this is the first device to separate natural mRNAs without using a d*A*/d*T* Watson−Crick-type interaction.

Introduction

Sequence analysis of messenger RNAs (mRNAs) is a key element in recombinant DNA techniques and gene engineering, because mRNAs directly code proteins.[2] Therefore, there is a persistent demand for simple and quick separation of pure mRNAs in scientific and industrial fields. The general procedure used for separating mRNAs is based on a method that cellular RNA mixtures (total RNA) are separated from cellular extract by the acid guanidine/phenol/chloroform method,[3] and mRNAs are separated from the total RNA with oligo(dT)-appended devices.[4] Since total RNA contains only 1−2% of mRNAs, a special procedure is necessary to separate such a scarce amount of mRNAs from total RNA. Most eukaryotic mRNAs have a poly(A) tail with 150−300 bases at the 3′ end, and selective recognition of the poly(A) tail thus makes it possible to separate mRNAs.[5−7] Oligo(dT)-appended cellulose columns, magnetic particles, or latex resins are used for this purpose in these days. These techniques can provide highly pure mRNAs, although there are some drawbacks. The oligo(dT) moiety is easily hydrolyzed both in vivo and in vitro and becomes expensive when attached to the device synthetically. If there is an alternative and inexpensive method, it should be very useful in many research fields.

Reagents that can recognize a specific sequence of polynucleotide are of significant importance in the gene engineering. This is usually achieved either by the formation of complimentary hydrogen bonds as in peptide-sustained nucleic acids[8,9] and amide-like *N*-pyrrole oligomers[10,11] or by the electrostatic interaction as in polyethyleneimine,[12,13] and cationic-glycoside.[14,15] As well as these reagents, schizophyllan (SPG) which is also a kind of polysaccharides can be used as a specific polynucleotide-receptor.[16−18] SPG is a natural polysaccharide produced on a large scale by fungus *Schizophyllum commune* of the *Basidiomycota*, and it can be supplied inexpensively (less than 1/1000 of oligo(dT)). The main chain consists of β-(1→3)-D-glucan and one β-(1→6)-D-glycosyl side chain links to the main chain every three glucose residues (Figure 1A).[19,20] In nature, three SPG chains form a triple stranded helix in water, and the helix is dissociated to the single stranded SPG (s-SPG) in dimethyl sulfoxide (DMSO).[21−23] When water is added to the DMSO solution, s-SPG collapses owing to the formation of hydrogen bonds.[24,25] Recently, we found that s-SPG forms a polymer complex with some single stranded polynucleotides with the hydrogen bonding and hydrophobic interactions.[16,17] One of the novel features in this complex is that the complexation occurs in a highly stoichiometric manner: that is, the stoichiometric analysis of the s-SPG/poly(C) complex indicates that two glucose units in the main chain are interacting with one cytosine unit.[17] Atomic force and scanning electron microscopy observations revealed that the complex adopts

* To whom correspondence should be addressed. Fax: (+81)-92-642-3611. Tel: (+81)-92-642-3585. E-mail: seijitcm@mbox.nc.kyushu-u.ac.jp.
† Fukuoka Industrial Technology Center.
‡ University of Kitakyushu.
§ Kyushu University.

10.1021/bm049623l CCC: $30.25
Published on Web 12/10/2004

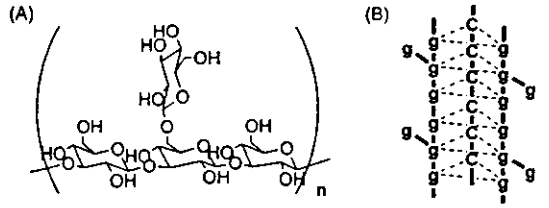

Figure 1. Chemical structure of schizophyllan (SPG) (A), and schematic illustration of the s-SPG/poly(C) complex (B). g and C denote the glucose and cytosine in the chains, respectively, and the dotted lines present the hydrogen bonds.

the same rodlike architecture as the original triple helix.[26] These lines of evidence indicate that the complex consists of the two s-SPG chains and one poly(C) chain to form a new triple helix, as illustrated in Figure 1B. Another novel feature is the specific selectivity of s-SPG for polynucleotides. In the case where homo-polynucleotides are mixed with s-SPG in salt free neutral water, the complexation occurs with poly(C), poly(A), poly(dA), and poly(dT) but not with poly(G), poly(dG), poly(dC), and poly(U).[17] This selectivity is governed by the difference of whether hydrogen-bonding sites of the polynucleotide are free or not. Poly(G), poly(dG), poly(dC), and poly(U) are inactive because of formation of a tetramer or a dimer. The hydrogen-bonding sites in these bases are used to form the intramolecular complex. In contrast, poly(C), poly(A), poly(dA), and poly(dT) do not form such an intramolecular complex and their hydrogen-bonding sites are unoccupied and available for the complexation.

Basic Concept and Strategy to Separate Native mRNAs

Our previous communication[27] reported that an s-SPG-appended column can trap only such RNAs that can form the complex with s-SPG (such as poly(C) and poly(A)) but elutes other RNAs which do not form the complex (such as poly(G)). Eukaryotic mRNAs have a poly(A) tail and we already know that s-SPG can bind poly(A) itself. These facts suggest that one can construct a separation device for mRNA using the s-SPG/poly(A) complexation. Our basic strategy consists of the following procedures (also schematically presented in Figure 2). It is known that to form the complex more than 30 homo-nucleotide sequences are necessary.[28] This means that most natural polynucleotides do not form the complex with s-SPG, except poly(A) tails in mRNA. When total RNA is added into an s-SPG-appended column with an appropriate solvent (loading solvent) which can allow poly(A) tails to bind s-SPG, mRNAs should be trapped by the s-SPG-appended column, whereas ribosomal RNAs (rRNAs) and transfer RNAs (tRNAs) should be eluted eventually. After the column is rinsed off to clean residual tRNAs and rRNAs with the loading solvent, only mRNAs should be left in the column. This pure mRNAs can be recovered by rinsing it with a "recovering solvent". This solvent can be hot water whose temperature is higher than the dissociation temperature[17] or an acidic solution in which protonation leads to dissociation of the complex.[29] In this work, we used Tris-HCl buffer (pH 7.5, 0.10 M) at 5 °C as

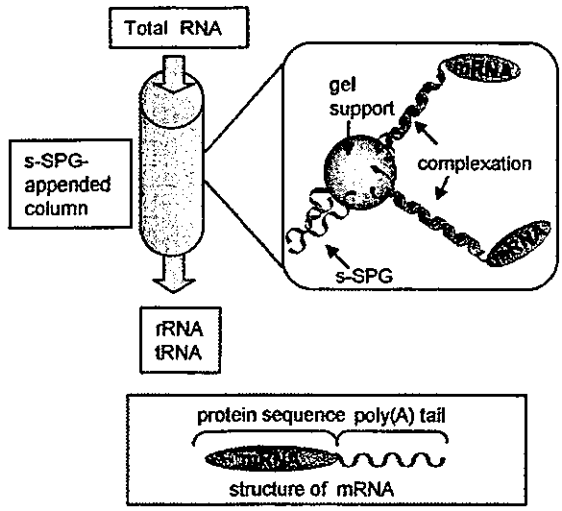

Figure 2. Our basic strategy to separate mRNAs with the s-SPG/poly(A) tail complexation. The s-SPG-appended column contains the gel support on which the s-SPG reducing terminals have been attached to the surface carboxyl groups. Eukaryotic mRNAs have a poly(A) tail and the s-SPG can bind to the tail. When total RNA is added into the column, rRNAs and tRNAs are eluted. The pure mRNAs can be recovered by rinsing with a "recovering solvent".

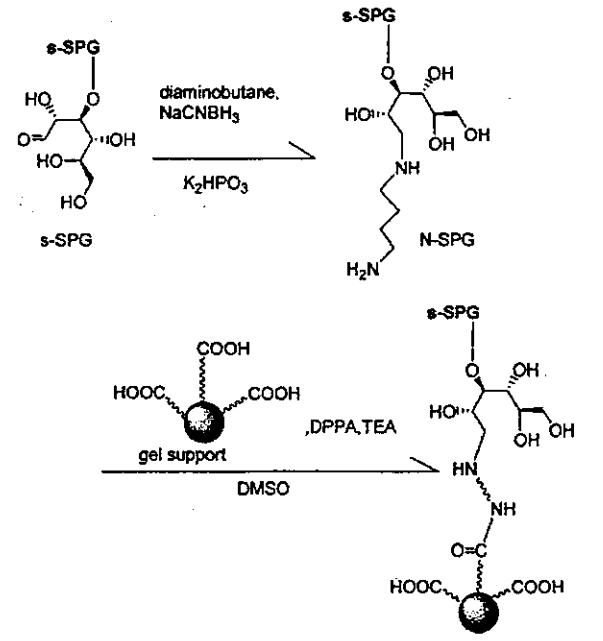

Figure 3. Synthesis scheme of the s-SPG-appended gel support.

the loading solvent and salt free neutral water at 70 °C as the recovering solvent.

Design of an s-SPG-appended column is the most important to avoid nonspecific interactions. To avoid the nonspecific interaction between polynucleotides and cations, we employed a carboxyl carrier gel support. Thus, we successfully introduced an amino group to the reducing terminal of s-SPG (see Figure 3).[30,31] The amino-terminated s-SPG was immobilized on the gel support in the presence of a condensing agent.

Experimental Section

Materials. SPG was kindly supplied by Taito Co. in Japan. The molecular weight and the number of repeating units were

evaluated to be 1.5×10^5 and 231, respectively.[21] Poly(C) and poly(A) were purchased from Amersham Biosciences and poly(G) from Wako Chemicals. Diaminobutane was purchased from Wako Chemicals and diphenyl phosphorazidate (DPPA) from Tokyo Chemical Industry. Sample solution and buffer were made of RNase free distilled water treated with dietyl pyrocarbonate (Nacalai Tesque). Total RNA was extracted from yeast (*saccharomyces cerevisiae* Kyokai No.7). The yeast was cultured in the YM Broth medium (Difco) for 18 h at 30 °C, and the total RNA was isolated by the acid guanidine/phenol/chloroform method using TRIzol reagent (Invitrogen). mRNAs were extracted from total RNA by using PolyATract mRNA Isolation System (Promega) following the instructions from the manufacturer.

Synthesis of Amino-Terminated s-SPG (N−SPG) and Preparation of s-SPG Column. Figure 3 presents our procedure to attach s-SPG chains to a gel support. First of all, we attached diaminobutane to the reducing terminal of s-SPG according to the following procedure. SPG (500 mg, 2.97×10^{-3} mol/glucose) was dissolved in 100 mL of 0.20 M K_2HPO_3 aqueous solution. Diaminobutane (100 mg, 1.13×10^{-3} mol) and sodium cyanoborohydride (100 mg, 1.59×10^{-3} mol) were added to the SPG solution four times every 6 h. Then the mixture was stirred for 26 h at 30 °C. After the mixture was dialyzed for 2 days with distilled water, the solvent was removed by a freeze-drying method. The introduction of diaminobutane into s-SPG was confirmed qualitatively by the ninhydrin reaction on a thin-layer chromatography plate. The diaminobutane-attached s-SPG was denoted by N-SPG.

N-SPG was reacted with carboxyl groups on a gel support with a coupling reaction using DPPA in DMSO as follows. AF-Carboxyl TOYOPEARL 650M (Tosoh) (18 g) was suspended into 100 mL of dehydrated DMSO. The mixture containing N-SPG (200 mg, 1.19×10^{-3} mol/glucose), triethylamine (45 mg, 4.44×10^{-4} mol), and DPPA (250 mg, 9.08×10^{-4} mol) was shaken for 48 h at 30 °C. Then the mixture was filtrated and the residue was washed with DMSO (50 mL x 3) and distilled water (50 mL x 3). The resultant s-SPG-appended gel support (9 mL) was packed into a plastic column with 15 mm in diameter and 40 mm in length (s-SPG column). As a reference, AF-Carboxyl TOYOPEARL 650M was packed into a column with 15 mm in diameter and 40 mm in length (blank column). It was difficult to estimate the amount of immobilized s-SPG on the gel support by the elemental analysis, because the mass fraction of the gel support is more than 99% and it is practically impossible to detect the N atom fraction.

Instead of the elemental analysis, we examined how much poly(C) was bound onto the gel support. According to our work,[17] poly(C) has the highest binding constant for s-SPG and the complexation takes place with the highest yield among polynucleotides. Therefore, we can measure (or have a semiquantitative value at least) how much s-SPG molecules are bound onto the support. The s-SPG column was washed in an excess amount of poly(C) solution under the loading conditions, and after 12 h, free poly(C) was removed by rinsing off the column with the loading solvent. The rinse of the column was repeated until there was no poly(C) detected by the UV measurement. The bound poly(C) was collected by rinsing the recovering solvent. In this experiment, the amount of poly(C) bound to the s-SPG column is estimated to be 8.2×10^{-6} mol/nucleotide from the UV measurement. If the stoichiometry (two glucose units in the s-SPG main chain with respect to one cytosine) is held even on the gel surface in the s-SPG column, the amount of s-SPG which is available for trapping RNAs on the gel is calculated to be 2.4×10^{-6} mol/glucose unit per 1 mL-gel(wet).

Separation of RNAs with s-SPG Column. After the s-SPG column was washed with the loading solvent, the solvent was exchanged for the RNA solution at 5 °C. The concentrations and volumes of the RNA solution were 1.25×10^{-3} M/nucleotide and 200 μL for poly(A) or poly(C), 7.09×10^{-5} M/nucleotide and 200 μL for mRNAs, and 2.88×10^{-4} M/nucleotide and 500 μL for total RNA. The elutes were monitored by following the absorbance at 260 nm on a UV-2200A UV−vis spectrophotometer (Shimadzu) with a 5.0×10 mm quartz cell.

Northern Blot Analysis of mRNAs. A total of 1.0 μL of RNA solutions fractionated were spotted onto a Hybond-N^+ nylon membrane (Amershame Biosciences). Oligo(dT)$_{18}$ was purchased from Bio Labs as a hybridization probe for mRNAs. Digoxigenin labeled oligo(dT)$_{18}$ (Dig-oligo(dT)) was prepared by using a DIG oligonucleotide tailing kit (Roche Diagnostics) according to the supplier's instructions. Dig-oligo(dT) was hybridized with mRNAs on the membrane for 12 h at 25 °C. mRNA/Dig-oligo(dT) hybrid was treated with an alkaline phosphatase-labeled Dig-antibody (Roche Diagnostics). The mRNA/Dig-oligo(dT)/alkaline phosphatase-labeled Dig-antibody ternary hybrid on the membrane was detected by using 4-nitro blue tetrazolium chloride (Roche Diagnostics) and 5-bromo-4-chloro-3-indolyl-phosphate (Roche Diagnostics).

Electrophoresis. SeaKem GTG agarose gel (Cambrex) was prepared at 1.5 wt % concentration with MOPS buffer, and formalin was electrophoresed for 25 min at 100 V. The migrants were stained with ethidium bromide. The migration patterns were revealed by UV irradiation and analyzed on a Typhoon 9200 phosphorimager (molecular dynamics, Amersham Pharmacia Biotech).

Reverse Transcription-PCR (RT-PCR). A total of 9.0 μL of RNA solution was reverse-transcribed into complimentary DNA (cDNA) using Thermo Script RT-PCR System (Invitrogen) with oligo(dT)$_{18}$ primer. Then 2.0 μL of the reverse transcription reactant was utilized for PCR amplification of cDNA fragments for TDH1 (sense primer, 5′-GCTATTAACGGTTTCGGTAGA-3′; antisense primer 5′-TCTACGGCAACAGAGGAG-3′; 833 bp PCR product) and ACTYEAST (sense primer, 5′-CTTCCCATCTATCGTCG-GTAG-3′; antisense primer 5′-TCTTATGCTGCTTTCAC-CAGG-3′; 1011 bp PCR product). The PCR reaction mixture contained 2 units of Taq DNA polymerase, PCR buffer, 2.0×10^{-4} M dNTP, 1.0 μL of sense and antisense primers in a total volume of 50 μL. PCR was performed for 40 cycles. Each cycle involved a 94 °C/1min denaturation step, a 55 °C/1min annealing step, and a 72 °C/1min polymerization

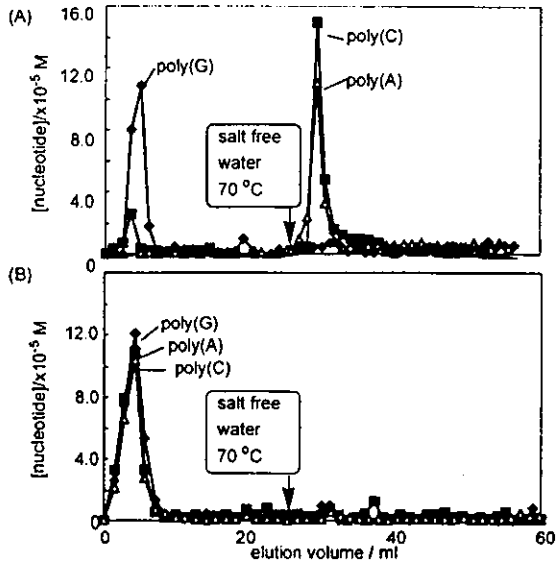

Figure 4. Comparison of the elution curves of homo-polynucleotides from the s-SPG column (A) and the blank column (B); poly(C) (■), poly(A) (△), poly(G) (◆).

step. The PCR products were electrophoresed on agarose gel and stained with ethidium bromide.

Results and Discussion

Molecular Recognition/Separation with s-SPG Column in Model Systems. Figure 4A compares elution curves among poly(C), poly(A), and poly(G) when they were loaded and subsequently recovered. As mentioned above, poly(C) and poly(A) can form the complex, but poly(G) cannot. As expected from these facts, elution of poly(C) or poly(A) was not observed under the loading conditions, and once the solvent was changed to the recovering conditions, they were eluted immediately. On the other hand, poly(G) was not trapped under the loading conditions. Figure 4B shows the elution curves when the exactly same polynucleotides and solvents were used for the blank column, to which no s-SPG had been attached. The column did not trap any polynucleotide under the loading conditions. These results indicate that poly(C) and poly(A) are retained in the s-SPG column through the complexation, not owing to nonspecific interactions such as ion-pair formation or physical adsorption. When we calculated the amount of the recovered poly(C) and poly(A), they were 93 and 97% of the fed polynucleotides, respectively. One can regard, therefore, that virtually 100% of poly(A) and poly(C) can be trapped in the column under the loading conditions and the recovering conditions can elute all bound polynucleotides.

We carried out the similar experiment under the same conditions as Figure 4, using a pure mRNAs sample obtained from yeast. Figure 5A plots the elution curve and panel B shows the northern dot blot for each fraction numbered in panel A. Although the S/N ratio is larger than that in Figure 4 owing to the lower concentration of mRNAs, there is no peak in the loading regime and a large absorption peak is clearly observed after changed to the recovering conditions. Panel B shows that this large peak contains mRNA at high concentrations. The present results indicate that the mRNAs

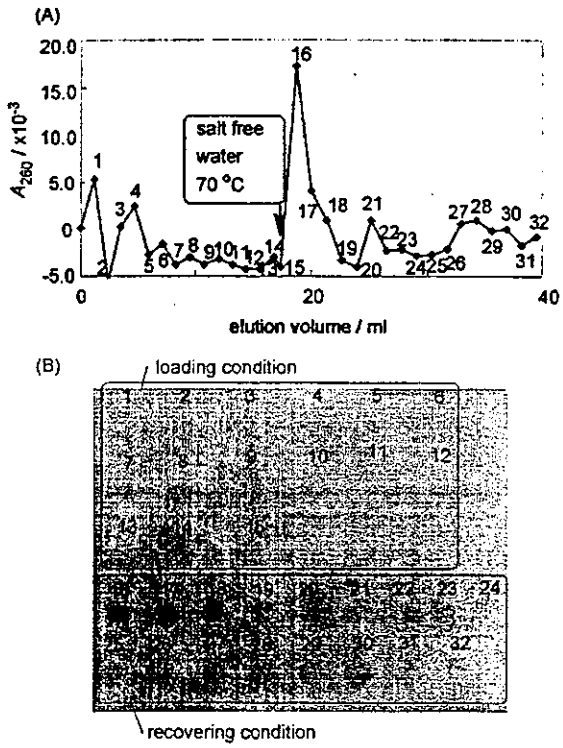

Figure 5. Elution curve of mRNAs from the s-SPG column (A) and the northern dot blot for all of the fractions (B).

elution is only observed for the 16−18th fractions. This result confirms that mRNAs can be trapped and recovered similarly to poly(A) and poly(C). The recovery rate is calculated to be about 90%.

The above two model experiments prove that our basic concept is valid and the s-SPG column can recognize the polynucleotides that can bind s-SPG in solution. Generally, one mRNA molecule consists of more than a few thousands bases and the poly(A) tail is just a small fraction of it. The present finding establishes that this tail length is sufficient for the s-SPG column to trap mRNAs.

Separation of mRNAs from Total RNA. Figure 6 shows the elution behavior of total RNA. Most of RNAs (more than 95%) are eluted immediately under the loading conditions. This feature is expected from the fact that total RNA contains only 1−2% of mRNAs and the residual components are rRNA and tRNA, which would not be trapped by the s-SPG column. After changed to the recovering conditions, a small amount of RNA is eluted. The northern dot blot (Figure 6, panel B) shows that mRNAs are not included in the major fraction at all but are concentrated in the 18th fraction. For comparison, Figure 7A shows the elution behavior for the blank column. The elution curve itself in the blank column exhibits the same feature, that is, the major elution in the 3/5 fractions and the minor elution after changed to the recovering conditions. However, a remarkable difference is observed for the northern blot analysis. In the blank column, mRNAs are included in the major fraction and the minor elution does not contain any mRNAs (Figure 7, panel B). This experiment demonstrates that the s-SPG column can separate a trace amount of mRNAs from total RNA owing to the s-SPG/mRNA complexation.

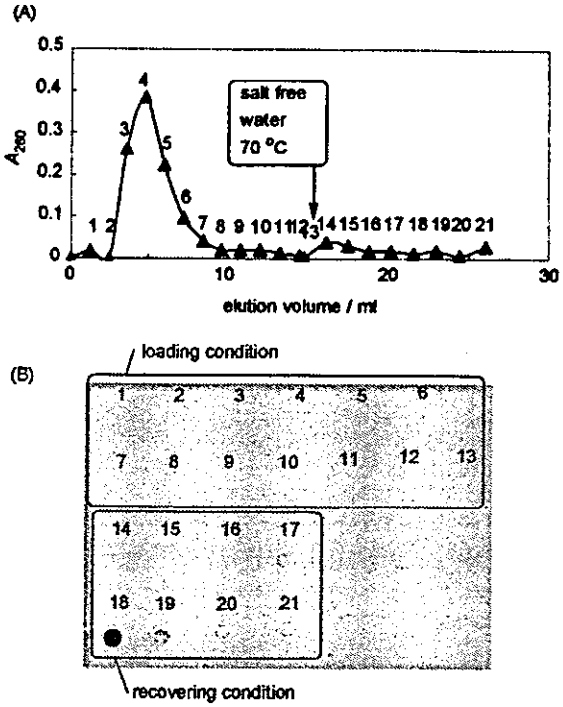

Figure 6. Elution curve of total RNA from the s-SPG column (A) and the northern dot blot for all the fractions (B).

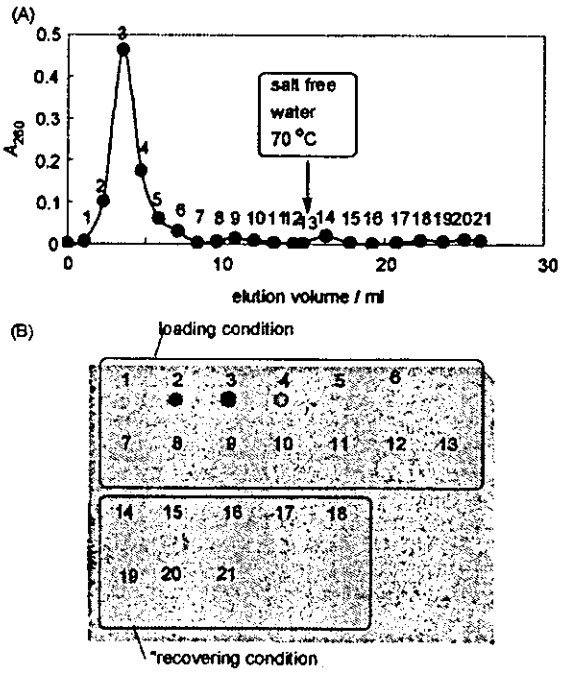

Figure 7. Elution curve of total RNA from the blank column (A) and the northern dot blot for all the fractions (B).

Purity of the Separated mRNAs Sample. Since mRNAs have a large distribution in the number of base pairs, the gel electrophoresis band is smeared, ranging from approximately 8.0 kb to 0.5 kb. On the other hand, 28 S rRNA, 18 S rRNA, and 5S rRNA appear as single clear bands, respectively.[32] Purity of the mRNAs separated by the s-SPG column was examined by agarose gel electrophoresis. Figure 8A compares the migration patterns between the total RNA and mRNAs samples. The pattern of total RNA in lane 1 is a typical one, having three 28 S rRNA, 18 S rRNA, and 5S

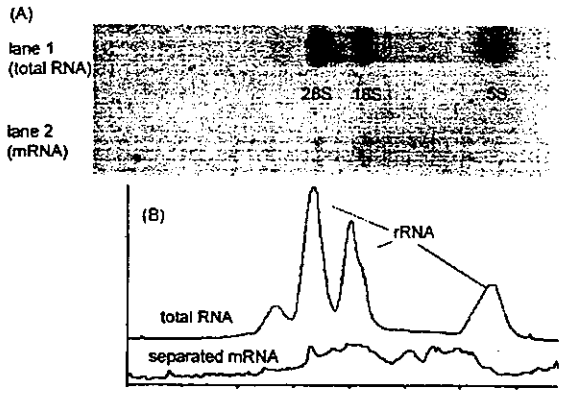

Figure 8. Comparison of the electrophoresis pattern among total RNA (lane1) and mRNAs separated by the s-SPG column (lane 2) (A) and the intensity profiles of lane 1 and lane 2 (B).

rRNA bands as indicated in the figures. On the other hand, when we examined the separated mRNAs, it showed a smear and weak band as presented in lane 2.

Using a densitometer, the intensity profiles of the lane 1 and lane 2 are plotted in Figure 8B. In the profile of lane 2, we can recognize small peaks due to rRNAs, overlapping with the mRNAs broad band. Applying a peak de-convolution technique, the peaks of rRNAs were subtracted from the original peak and the purity of mRNAs was estimated to be 87%. In these days, the oligo(dT)-appended latex deposited on the spin-column has been commercialized as a mRNAs separation kit. The application of this kit according to the recommended recipe to the present system showed that the purity of isolated mRNAs is 66−79%. It indicates that the s-SPG column can separate mRNAs in higher purity than the oligo(dT)-appended latex system.

We demonstrated to confirm that the separated mRNAs could be used for RT-PCR. If most of the isolated mRNAs are not cleaved in the separation process, the mRNAs should be reverse-transcribed into cDNAs by using the oligo$(dT)_{18}$ primer. Then, it would be possible to amplify an optional sequence from the cDNAs mixture. In this work, ACTYEAST (1011 bp) and TDH1 (833 bp) sequences were amplified in the cDNAs mixture. Since ACTYEAST and TDH1 are expressed constantly in a yeast cell, they can be regarded as a representative system of all mRNAs. Figure 9 shows the electrophoresis pattern of the RT-PCR products from the separated mRNAs sample. It is clearly seen from Figure 9 that the single DNA product of about 1000 base pairs appears in both experiments of ACTYEAST and TDH1. These results support the view that the mRNAs separated in the s-SPG column is available for gene engineering.

Conclusions

In this paper, the s-SPG-appended column was prepared and applied to a separation system containing various RNAs. We demonstrated that the s-SPG column can trap only RNAs which form the complex with s-SPG. Also important is the finding that natural mRNAs are trapped in the s-SPG column by the s-SPG/poly(A) tail complexation. This result proves that s-SPG can form the complex not only with artificial homo-polynucleotides but also natural mRNAs. Furthermore,

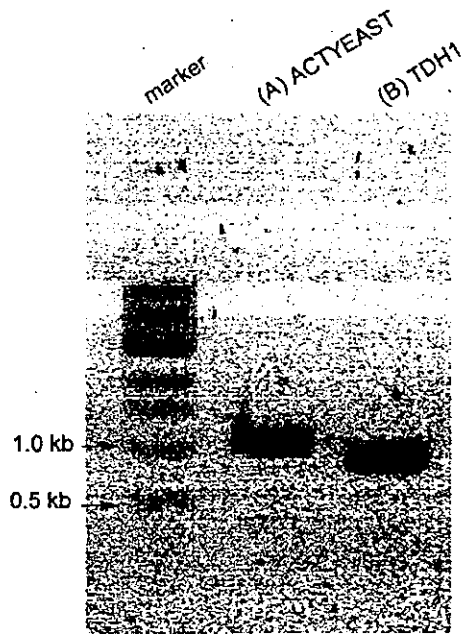

Figure 9. Electrophoresis patterns of RT-PCR products from mRNAs separated by the s-SPG column. ACTYEAST sequence (A), TDH1 sequence (B).

we succeeded in separating mRNAs from total RNA by using this s-SPG-appended column. This fact indicates that s-SPG/mRNA complexation occurs with high selectivity even in the RNA mixture. It should be emphasized that this separation system consists of only a neutral polysaccharide, but not of nucleobases at all. As far as we know, this is the first example to recognize and separate natural mRNAs by using polysaccharide-polynucleotide complexation.

Acknowledgment. We thank Taito Co. in Japan for kindly providing the SPG sample. This work has been financially supported by SORST program of Japan Science and Technology Agency.

References and Notes

(1) This is the 33rd paper in the series of "Polysaccharide-Polynucleotide Complexes" and a related work has been presented in the 29th Symposium on Nucleic Acid Chemistry in Japan (Kimura, T.; Koumoto, K.; Mizu, M.; Kobayashi, R.; Sakurai, K.; Shinkai, S. *Nucl. Acids Res. Suppl.* **2001**, *1*, 283 and Kimura, T.; Sakurai, K.; Shinkai, S. *Kobunshikako* **2003**, *52*, 201−206).
(2) Alberts, B.; Johnson, A.; Lewis, J.; Raff, M.; Roberts, K.; Walter, P. *Molecular Biology of the Cell*, 4th ed.; Garland Science: New York, 2002.
(3) Chomczynski, P.; Sacchi, N. *Anal. Biochem.* **1987**, *162*, 156−159.
(4) Aviv, H.; Leder, P. *Proc. Natl. Acad. Sci. U.S.A.* **1972**, *69*, 1408−1412.
(5) Darnell, J. E.; Wall, R.; Tushinski, R. J. *Proc. Natl. Acad. Sci. U.S.A.* **1971**, *68*, 1321−1325.
(6) Lee, S. Y.; Mendecki, J.; Brawerman, G. *Proc. Natl. Acad. Sci. U.S.A.* **1971**, *68*, 1331−1335.
(7) Edmonds, M.; Vaughan, M. H.; Nakazato, H. *Proc. Natl. Acad. Sci. U.S.A.* **1971**, *68*, 1336−1340.
(8) Egholm, M.; Buchardt, O.; Christensen, L.; Behrens, C.; Freier, S. M.; Driver, D. A.; Berg, R. H.; Kim, S. K.; Norden, B.; Nielsen, P. E. *Nature* **1993**, *365*, 566−568.
(9) Kushon, S. A.; Jordan, J. P.; Seifert, J. L.; Nielsen, H.; Nielsen, P. E.; Armitage, B. A. *J. Am. Chem. Soc.* **2001**, *123*, 10805−10813.
(10) Gottesfeld, J. M.; Neely, L.; Trauger, J. W.; Baird, E. E.; Dervan, P. B. *Nature* **1999**, *387*, 202−205.
(11) Kerstien, A. T. P.; Dervan, P. B. *J. Am. Chem. Soc.* **2003**, *125*, 15811−15821.
(12) Bettinger, T.; Remy, J. S.; Erbacher, P. *Bioconjugate Chem.* **1999**, *10*, 558−561.
(13) Goula, D.; Remy, J. S.; Erbacher, P.; Wasowicz, M.; Levi, G.; Abdallah, B.; Demeneix, B. A. *Gene Ther.* **1998**, *5*, 712−717.
(14) Kiang, T.; Wen, J.; Lim, H. W.; Leong, K. W. *Biomaterials* **2004**, *25*, 5293−5301.
(15) Walter, F.; Vicens, Q.; Westhof, E. *Curr. Opin. Chem. Biol.* **1999**, *3*, 694−704.
(16) Sakurai, K.; Shinkai, S. *J. Am. Chem. Soc.* **2000**, *122*, 4520−4521.
(17) Sakurai, K.; Mizu, M.; Shinkai, S. *Biomacromolecules* **2001**, *2*, 641−650.
(18) Kimura, T.; Koumoto, M.; Sakurai, K.; Shinkai, S. *Chem. Lett.* **2000**, 1242−1243.
(19) Tabata, K.; Ito, W.; Kojima, T.; Kawabata, S.; Misaki, A. *Carbohydr. Res.* **1981**, *89*, 121−135.
(20) Tabata, K.; Itoh, W.; Hirata, A.; Sugawara, I.; Mori, S. *Agric. Biol. Chem.* **1990**, *54*, 1953−1959.
(21) Norisuye, T.; Yanaki, T.; Fujita, H. *J. Polym. Sci., Polym. Phys. Ed.* **1980**, *18*, 547−558.
(22) Sato, T.; Norisuye, T.; Fujita, H. *Macromolecules* **1983**, *16*, 185−189.
(23) Yanaki, T.; Norisuye, T.; Fujita, H. *Macromolecules* **1980**, *13*, 1462−1466.
(24) Sato, S.; Sakurai, K.; Norisuye, T.; Fujita, H. *Polym. J.* **1983**, *15*, 87−92.
(25) McIntire, T. M.; Brant, D. A. *J. Am. Chem. Soc.* **1998**, *120*, 6909−6919.
(26) Bae, A.; Lee, S.; Ikeda, M.; Sano, M.; Shinkai, S.; Sakurai, K. *Carbohydr. Res.* **2004**, *339*, 251−258.
(27) Kimura, T.; Koumoto, K.; Mizu, M.; Sakurai, K.; Shinkai, S. *Chem. Lett.* **2002**, 1240−1241.
(28) Koumoto, K.; Kimura, T.; Mizu, M.; Kunitake, T.; Sakurai, K.; Shinkai, S. *J. Chem. Soc., Perkin Trans. 1* **2002**, 2477−2484.
(29) Sakurai, K.; Iguchi, R.; Mizu, M.; Koumoto, K.; Shinkai, S. *Bioorg. Chem.* **2003**, *31*, 216−226.
(30) Koumoto, K.; Kimura, T.; Mizu, M.; Sakurai, K.; Shinkai, S. *Chem. Commun.* **2001**, 1962−1963.
(31) Matsumoto, T.; Numata, M.; Mizu, M.; Koumoto, K. Anada, T.; Sakurai, K.; Nagasaki, T.; Shinkai, S. *Biochim. Biophys. Acta* **2004**, *1670*, 91−104.
(32) Tsukagaki, A. *Experimental Medicine* **1988**, *17*, 2065−2068.

BM049623L

Composite Interfaces, Vol. 10, No. 4-5, pp. 489-504 (2003)

Also available online - www.vsppub.com

Fabrication and characterization of multi-component organosilane nanofilms

ATSUSHI TAKAHARA*, HIROKI SAKATA, MASAMICHI MORITA, TOMOYUKI KOGA and HIDEYUKI OTSUKA

Institute for Materials Chemistry and Engineering, Kyushu University, Hakozaki, Higashi-ku, Fukuoka 812-8581, Japan

Received 12 December 2002; accepted 25 March 2003

Abstract—Multi-component micropatterned organosilane monolayers are fabricated on a Si-wafer substrate by stepwise site-specific vacuum ultraviolet (VUV)-ray photodecomposition and chemisorption. The introduction of different organosilane components is confirmed by X-ray photoelectron spectroscopy (XPS). Atomic force microscopic and lateral force microscopic observations reveal that the line-widths of the micropatterned surface correspond to those of the photomask. Contact angle measurement reveals that the micropatterning of the surface functional groups influences the magnitudes of surface free energy. A line pattern with high wetting contrast shows anisotropic water condensing behavior. Also, the patterned surface is used for the site-specific polymerization and site-specific adsorption of microparticles.

Keywords: Organosilane; photodecomposition; chemisorption; patterning; surface nanostructure; surface properties; microparticle; polymer ultrathin film.

1. INTRODUCTION

Fabricating micro- and nano-devices using a bottom-up approach requires building blocks with a precisely controlled and tunable chemical composition, morphology, and size that can be fabricated virtually at will. Organosilane monolayer is a candidate for such building blocks because of its stability and ease of fabrication. As the silanol groups of organosilane monolayer prepared from organotrichlorosilane or organotrialkoxysilane strongly interact with the substrate surface, the monolayer is thermally and chemically robust compared with conventional amphiphilic

*To whom correspondence should be addressed. E-mail: takahara@cstf.kyushu-u.ac.jp

monolayers. Since the chain length of organosilane is approximately 1–3 nm, the organosilane forms a 'nanofilm' on the substrate surface. Organosilane monolayers, which have surfaces terminated by various functional groups, are useful for the manipulation of physicochemical properties of solid surfaces such as wettability [1], nanotribology [2], and protein adsorption behavior [3, 4]. A key to fabricating functional organosilane monolayers is controlling the distribution of surface functional groups [5–12]. Patterned microfeatures of organosilane monolayers can be fabricated on the substrate, allowing surface physicochemical properties to be area-selectively controlled. Photolithography has been developed as a micropatterning technique for organosilane monolayers [13, 14]. In the case of an ultraviolet (UV) source with $\lambda = 190–220$ nm, the oxidation reaction of the terminal group gives a carboxyl-terminated surface. On the other hand, in the case of a vacuum ultraviolet (VUV) source with $\lambda = 172$ nm, photodecomposition of the organic moiety occurs due to the higher photon energy of the VUV-ray compared with the bond energy of a typical C—C linkage. When VUV photodecomposition was applied to an organosilane monolayer in combination with chemical vapor adsorption (CVA) [15–18], which is the chemisorption technique for preparing the organosilane monolayers, this process enables easy fabrication of organosilane monolayer micropatterns [13, 19]. Using photolithography, one can prepare a micropatterned surface with various organosilane monolayers by repeating the photodecomposition and chemisorption processes. By changing the shape and area-ratio of the patterns

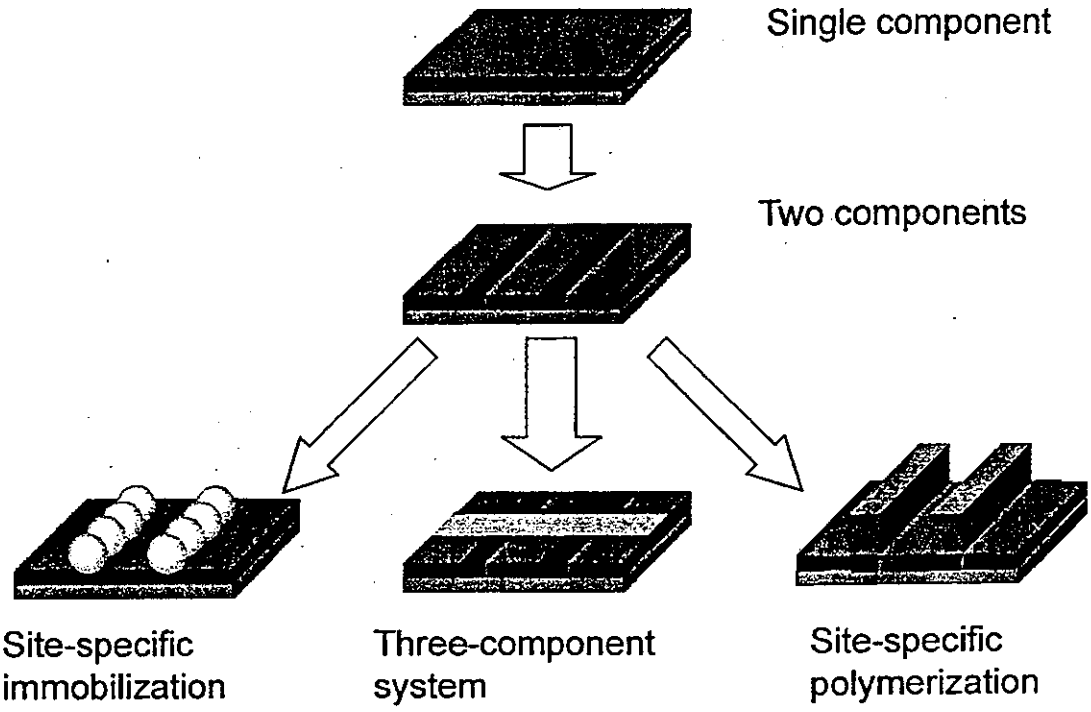

Figure 1. Schematic representation of surface patterning, site-specific polymerization, and site-specific immobilization of microparticles.

of the photomask, this technique enables one to control the area ratio and wettability gap of different organosilane monolayers.

A structural surface that exhibits patterns of varying wettability can be produced by chemisorption and local photodecomposition of organosilanes. Use of such patterns as templates for three-dimensional structures with various topographic and surface properties appears very promising. Site-specific adsorption of microparticles can be achieved by specific interaction between microparticles and a monolayer surface. The immobilization of a polymerization initiator on a functional monolayer enables site-specific polymerization, which can result in a large topography change. Figure 1 summarizes the scheme of micropatterning of organosilane monolayers, site-specific polymerization, and immobilization of microparticles on patterned organosilane monolayers. Those three processes are described in this paper.

In this study, we fabricated two- and three-component micropatterned organosilane monolayers (nanofilms) on silicon wafer surfaces by VUV photodecomposition in combination with chemisorption. The changes in surface chemical composition and physicochemical properties were characterized by X-ray photoelectron spectroscopy (XPS), contact angle measurements, and scanning force microscopy (SFM). Also, the patterned surface was applied for the site-specific atom transfer radical polymerization (ATRP) of methacrylate monomer and site-specific adsorption of charged microparticles.

2. EXPERIMENTAL

2.1. Fabrication of multi-component organosilane monolayers

Figure 2 shows the chemical structures of organosilane molecules used for the preparation of monolayers, including *n*-octadecyltriethoxysilane (OTES, Chisso), [2-perfluorohexyl]ethyltriethoxysilane (FHETES, Gelest), and N-[2-aminoethyl]-3-aminopropylmethyldimethoxysilane (AEAPDMS, Chisso). These organosilanes were used without further purification. Figure 3 outlines the essential steps used

Alkylsilane

$CH_3(CH_2)_{17}Si(OC_2H_5)_3$

n-octadecyltriethoxysilane(OTES:$C_{18}Si$)

Fluoroalkylsilane

$CF_3(CF_2)_5(CH_2)_2Si(OC_2H_5)_3$

[2-(perfluorohexyl)ethyl]triethoxysilane(FHETES:$C^F_6C_2Si$)

Aminosilane

$NH_2(CH_2)_2NH(CH_2)_3SiCH_3(OCH_3)_2$

N-(2-aminoethyl)-3-aminopropylmethydimethoxysilane

(AEAPDMS : NC_2NC_3 SiC)

Figure 2. Chemical structure of organosilanes.

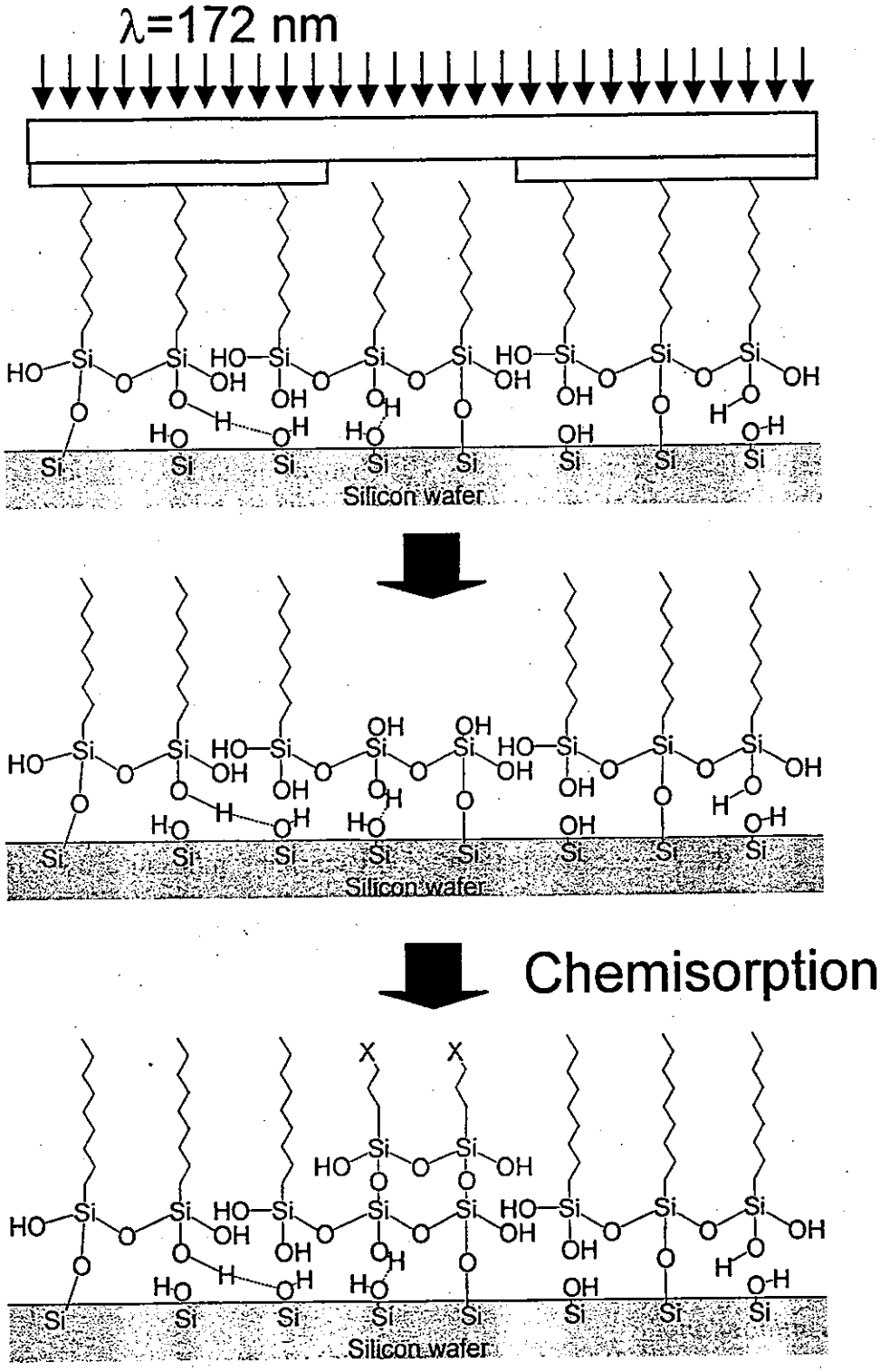

Figure 3. Schematic representation of site-specific photodecomposition by irradiation with VUV ray and chemisorption.

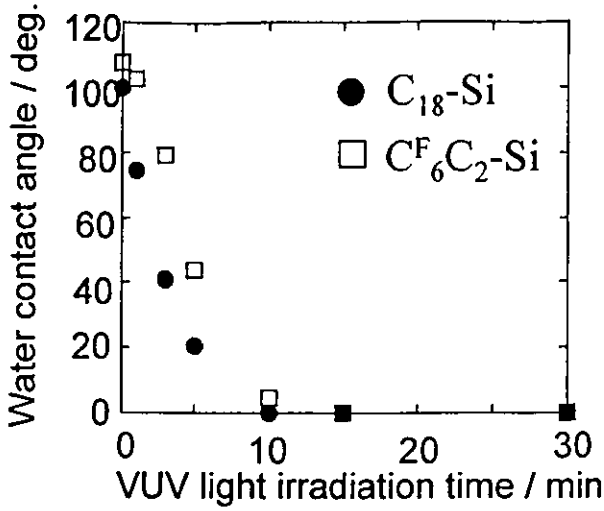

Figure 4. Variations of water contact angle of OTES and FHETES monolayers with VUV irradiation time.

in fabricating micropatterned organosilane monolayers. The first step was the preparation of organosilane-grafted Si-wafer substrates, beginning with polished n-type Si(111) wafers with 0.5 mm thickness. These were immersed in a H_2SO_4/30% H_2O_2 aq. (70/30 v/v) mixture at 373 K for 1 h to obtain the Si−OH terminated surface, which immobilizes organosilane molecules [21, 22]. Substrates were photochemically cleaned by a VUV/ozone treatment under 15 mmHg for 10 min, so as to completely decompose the organic contaminant before preparation of the first organosilane monolayer [14, 20], which in this case was OTES (molecular length is *ca.* 2.3 nm) [20]. We used the CVA method to fabricate the monolayers [16, 17]. The cleaned Si wafers were placed together with a glass cup filled with 0.2 cm^3 OTES liquid into a Teflon™ container. The container was sealed with a screw top and placed in an oven maintained at 423 K for 3 h. A uniform monolayer formation was confirmed by atomic force microscopic (AFM) observation.

Removal of the monolayer in selected areas by photodecomposition was the next step in the process. In photolithography, irradiation with VUV-ray (λ = 172 nm) leads to excitation cleavage of covalent bonds, such as C−C, C−H, and Si−C bonds, and formation of surface Si−OH residues [14]. Figure 4 shows the variation of water contact angle on OTES and FHETES monolayers with the irradiation time of VUV-ray generated from an excimer lamp (Ushio Electric, UER 20-172V, λ = 172 nm). VUV irradiation was carried out under 0.8 mmHg of pressure. Initially, OTES and FHETES monolayers gave water contact angles larger than 100 deg. However, within 15 min, the angles approached 0 deg, which indicates that almost complete removal of a monolayer can be achieved with 15 min irradiation of VUV-ray. The monolayer removal was also confirmed by XPS measurement.

Using a photomask, one can prepare a pattern with the desired shape and precisely controlled arrangement of surface functional groups. The OTES grafted Si-wafers were placed in a vacuum chamber evacuated by a rotary pump. The pressure in

the chamber was maintained under 0.8 mmHg. The sample was then covered with a photomask (Toyo Precision Parts MFG) in preparation for irradiation. The photomask consisted of a 2 mm-thick quartz glass plate with a 0.1 μm-thick Cr pattern; a cylindrical stainless steel weight placed on the photomask ensured satisfactory contact between the sample surface and the mask. The sample was irradiated for 15 min with VUV light. To remove the decomposed residue of the organosilane monolayers, the patterned sample was sonicated for 10 min in ethanol and dried *in vacuo*. The second organosilane monolayer, FHETES (molecular length is *ca.* 1.0 nm), was then introduced into the first patterned surfaces by a similar method with OTES.

The formation of a ternary component monolayer requires another photodecomposition and chemisorption process, with the photomask rotated 90 degrees from its position in the first patterning step. The OTES/FHETES sample was then irradiated for 20 min with VUV, resulting in cross-line micropatterns on the substrate surfaces. The third organosilane monolayer, AEAPDMS (molecular length is *ca.* 0.9 nm), was finally introduced into the second-patterned substrate surfaces, again by the CVA method.

2.2. *Characterization of multi-phase organosilane monolayers*

Surface free energy of the monolayer was evaluated from the contact angles of the water and the methylene iodide droplets at 298 K based on Owens and Wendt's method [23].

The stepwise fabrication of three-component organosilane monolayer was confirmed by X-ray photoelectron spectroscopy (XPS) with Phi ESCA 5800 system (Physical Electronics). The XPS measurement was performed with a monochromatized Al K_α X-ray source at 14 kV and 24 mA. The emission angle of photoelectrons was set to be 45 deg.

A Physical Electronics TRIFT-II time-of-flight secondary ion mass spectroscopic (ToF SIMS) instrument (Ulvac Phi) was used to make the SIMS imaging. Negative ion images were obtained with a 15 kV primary pulsed Ga^+ ion beam (pulse width of 13 ns) with a 2 nA beam current. The scan area was 100 μm $\times$ 100 μm.

The surface nanostructure and frictional properties of the micropatterned monolayer were investigated by atomic force microscopic (AFM) observation and lateral force microscopic (LFM) measurement. AFM and LFM images were obtained with TMX-2100 (Vecco) under constant force mode in air at 300 K with 50–60% relative humidity, using a 100 μm $\times$ 100 μm scanner and a Si_3N_4 tip on a triangle cantilever with a spring constant of 0.032 N m^{-1}.

The formation of droplets of water on the micropatterned surface was observed with an environmental scanning electron microscope (XL30 ESEM, Philips). At first, the ESEM sample chamber was evacuated below the saturated vapor pressure (612 Pa) of water at 273 K. Then, the sample surface was cooled to 273 K and the vapor pressure of the ESEM sample chamber was increased to 700 Pa.

3. RESULTS AND DISCUSSION

3.1. Characterization of multi-phase organosilane monolayers

We used XPS and contact angle measurements to characterize the changes in the surface chemical compositions of the micropatterned organosilane monolayers. Figure 5 shows the XPS survey scan spectra of the changes in the surface chemical compositions through the micropatterning process. The OTES monolayer showed C_{1s}, O_{1s}, Si_{2s}, and Si_{2p} peaks at 285, 533, 151, and 100 eV, respectively [21]. The OTES/FHETES patterned Si substrate clearly showed an additional F_{1s} peak at 690 eV, while the OTES/FHETES/AEAPDMS grafted Si substrates showed another N_{1s} peak at 400 eV [21]. The decomposition of the FHETES monolayer was revealed from the decreased intensity of the F_{1s} peak. The grafting of organosilane monolayers was also confirmed from C_{1s} and N_{1s} XPS narrow scan spectra. These results indicated that the three kinds of organosilane molecules were subsequently grafted on the substrate surfaces.

Local photodecomposition of the organosilane monolayer was also confirmed by ToF-SIMS. The FHETMS monolayer was irradiated with VUV-ray through a photomask, and the secondary ion image was measured. Figure 6 shows F^- ($m/z = 18.987-18.99$) and SiO_2^- ($m/z = 59.84-59.88$) in a secondary ion image FHETMS monolayer irradiated with VUV-ray under a photomask. F^- originated from the fluorine group of the fluoroalkyl chain, and SiO_2^- originated from the native

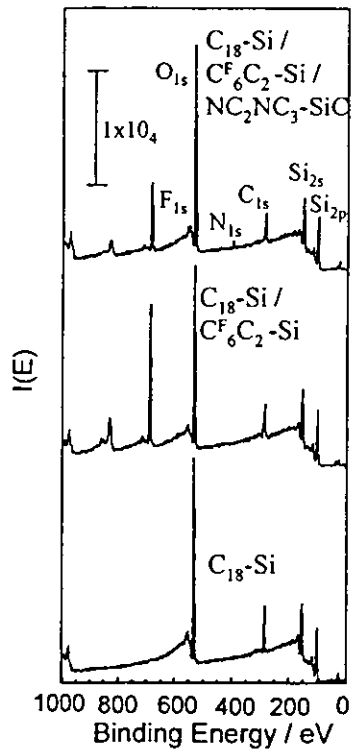

Figure 5. XPS survey scan spectra of the OTES, OTES/FHETES, and OTES/FHETES/AEAPDMS micropatterned Si substrates (emission angle is 45 deg).

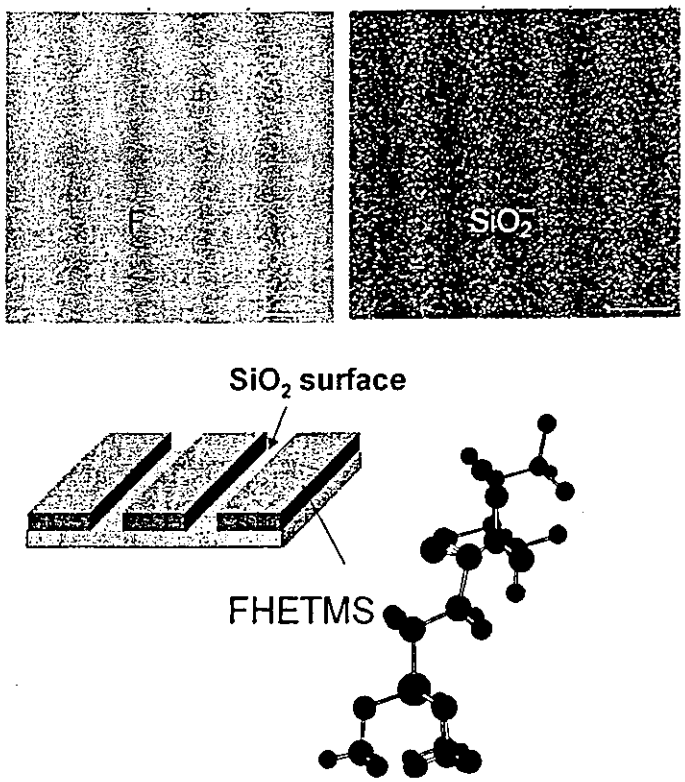

Figure 6. Time-of-flight secondary ion spectroscopic images of F^- (m/z = 18.987–18.99) and SiO_2^- (m/z = 59.884–59.88) ion of a partially photodecomposed FHETMS monolayer.

oxide layer of the Si-wafer substrate. In spite of the large diameter (*ca.* 300 nm) of the Ga ion beam, a line pattern was clearly observed. Since F^- was not observed from the region where SiO^- showed strong intensity, the removal of the monolayer by irradiation with VUV-ray was confirmed.

The first step of the fabrication of a multi-component monolayer is the preparation of a two-component system. Figures 7a and 7b show atomic force microscopic (AFM) and lateral force microscopic (LFM) images of a two-component micropatterned organosilane monolayer, respectively. Figure 7c shows the line profile of the white line in Fig. 7a. AFM and LFM images show line-pattern microstructures fabricated on the Si-wafer substrates. The widths of the fabricated FHETES lines were consistent with the widths of slits in the photomask. In the line profile of the AFM image shown in Fig. 7c, the height difference between the OTES and FHETES surfaces was *ca.* 1.4 nm. The height difference corresponds to the difference in the molecular length (*ca.* 1.3 nm) between OTES and FHETES. The LFM image shows the contrast due to the difference in physical properties of monolayer components. The FHETES-grafted areas showed a higher magnitude of lateral force values in comparison with the OTES-grafted ones, owing to the larger shear strength of the rigid fluoroalkyl chain of the FHETES chains [2].

Successful fabrication of a micropattern with three kinds of functional groups was confirmed by SFM observation. Figures 8a and 8b show AFM and LFM

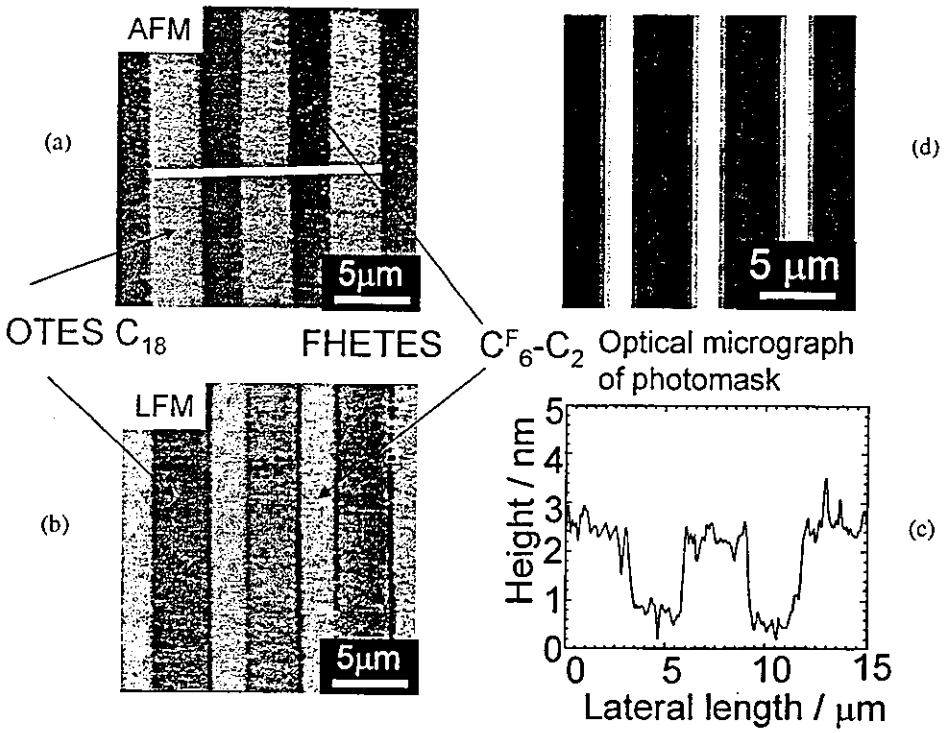

Figure 7. (a) AFM and (b) LFM images and (c) AFM height profile of a two-component line-patterned (OTES/FHETS) organosilane monolayer. (d) An optical micrograph of the photomask used is also shown.

images of a three-component micropatterned organosilane monolayer, respectively. Figures 8c and 8d show the line profiles of the white lines in Fig. 8a. These figures show cross-line microstructures fabricated on Si-wafer substrates. The widths of the fabricated FHETES and AEAPDMS lines were consistent with the widths of slits in the photomask. In the line profile of the AFM image shown in Fig. 8c, the height difference between the OTES and FHETES surfaces was *ca.* 1.4 nm. The height difference corresponds to the difference in the molecular length (*ca.* 1.3 nm) between OTES and FHETES. On the other hand, the height difference between the OTES and AEAPDMS surfaces was *ca.* 1.5 nm (Fig. 8d), corresponding to the difference in the molecular length (*ca.* 1.4 nm) between OTES and AEAPDMS. The origin of the contrast in the LFM image is explained by the difference in surface properties of three components, i.e. the chain rigidity, crystallinity, and chemistry of terminal functional groups of the organosilane molecules [24]. AEAPDMS-grafted areas are the brightest of the three components, because the terminal amino groups exerted high lateral force due to the strong interaction between the hydrophilic amino group and the Si—OH group of the cantilever tip. The area ratio of the prepared micropatterned monolayer is in accord with that of the target value, i.e. the estimated area ratio of OTES/FHETES/AEAPDMS was 4 : 2 : 3.

Changes of surface functional groups by micropatterning were also reflected in the magnitude of surface free energy. Table 1 shows the surface free energies of uniform or micropatterned organosilane monolayers. The surface free energy

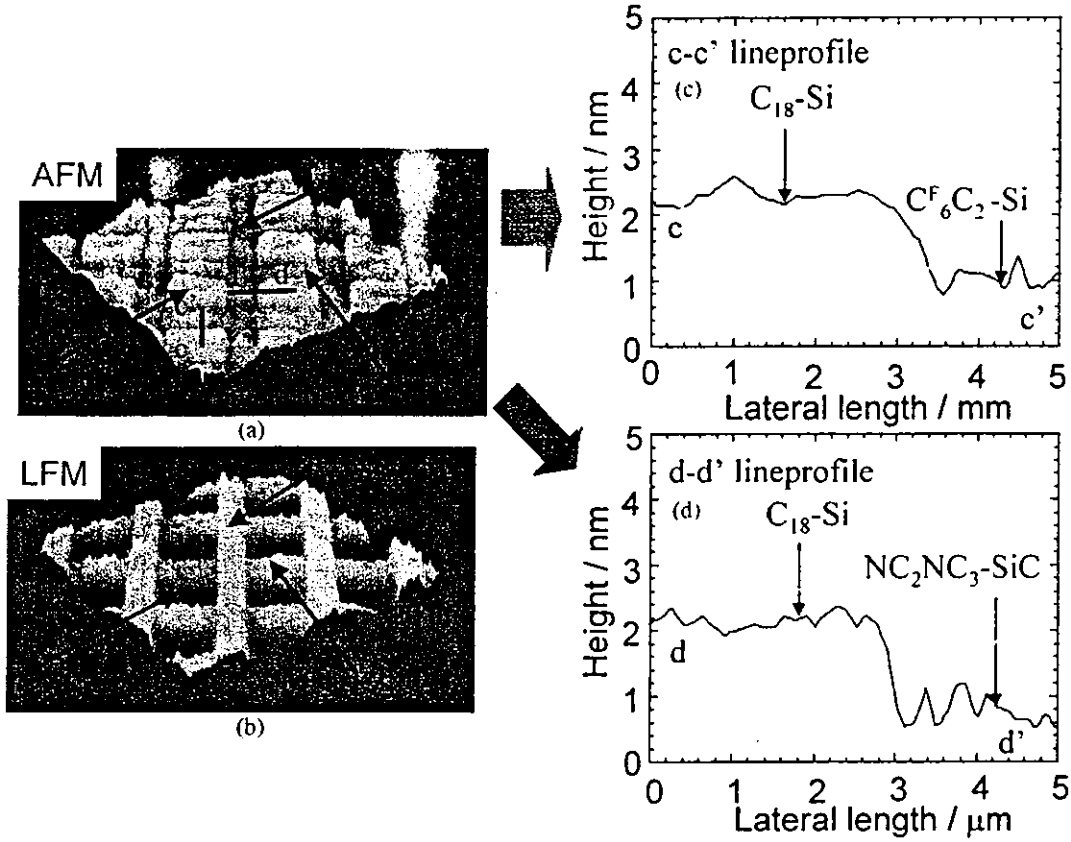

Figure 8. AFM and LFM images of three-component micropatterned organosilane monolayers. (a) AFM image of an OTES/FHETES/AEAPDMS micropatterned surface; (b) LFM image of an OTES/FHETES/AEAPDMS micropatterned surface; (c), (d) line profiles of white line parts in (a).

Table 1.
Surface free energy of micropatterned organosilane monolayers

Organosilanes	γ_{sv}/mJ m^{-2}	γ_{sv}^{d}/mJ m^{-2}	γ_{sv}^{h}/mJ m^{-2}
AEAPDMS	48.5	34.3	14.2
OTES	20.1	18.1	2
FHETES	14.7	13.1	1.6
OTES/FHETES	17.1	15.5	1.6
OTES/FHETES/AEAPDMS	23.8	19.7	4.1

was calculated from the contact angles of water and methylene iodide based on Owens and Wendt's method [24]. In the table, γ_s^d and γ_s^h denote the dispersion and hydrogen-bonding components of surface free energy, respectively. The surface free energy of the OTES/FHETES micropatterned surface is smaller than that of the OTES monolayer surface; the decrease can be attributed to the fluoroalkyl groups of FHETES, which are known to decrease surface free energy [7]. On the other hand, the surface free energy, especially the hydrogen-bonding component γ_s^h, extensively increased after the grafting of AEAPDMS; this increase was attributed

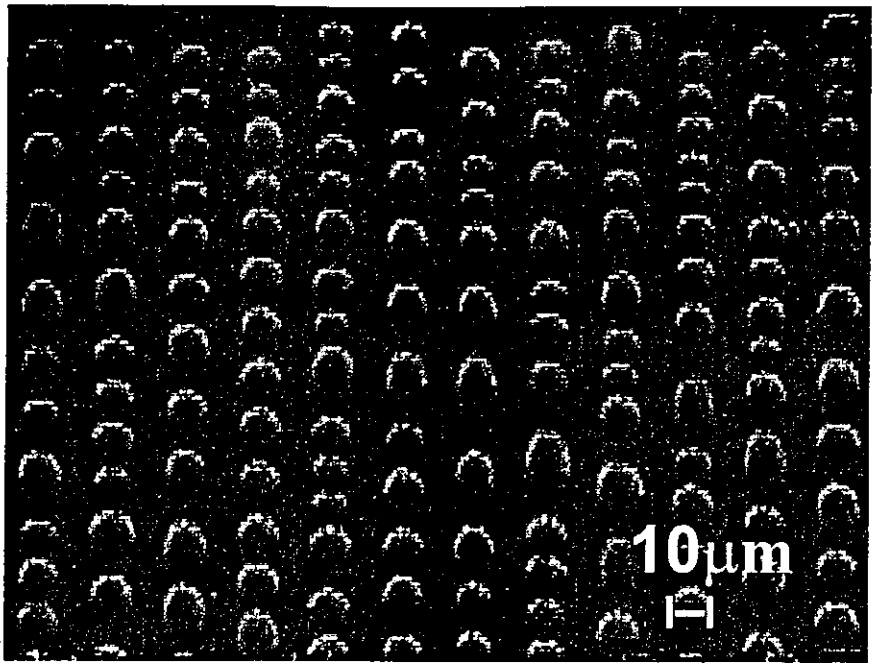

Figure 9. Environmental scanning electron microscopic image of water droplet on a monolayer after exposure to water vapor at 273 K.

to the relatively high polarity of amino groups introduced in the grafted AEAPDMS monolayers [24]. Taken together with the SFM observation, this stepwise change of surface free energy confirmed that the three-component organosilane surfaces had been micropatterned with highly hydrophobic, hydrophobic, and hydrophilic areas, respectively. Our patterning of three-component organosilane monolayers is expected to be a useful template for immobilizing various organic or inorganic materials on Si surfaces.

A laterally structured surface with different wetting properties may be produced by various techniques such as microcontact printing [25], micromachining [26], photolithography [27], and vapor deposition [28]. If one phase of a micropatterned surface has an affinity towards a certain liquid, the surface can be utilized as a template for local liquid condensation. We prepared a line-patterned high wettability contrast surface via the local photodecomposition of a FHETMS monolayer. The advantage of this method is that the height difference of the two phases is less than 2 nm. Figure 9 shows the ESEM image of the water droplet on the surface of the FHETMS/Si−OH patterned monolayer during the initial condensation process. The water started to condense on the Si−OH part of the patterned surface. The size of the water droplet and the number of water droplets increased until the droplets coalesced in a line. Since water has large surface free energy compared with the FHETMS phase, the water is more likely to condense on the higher surface free energy region. After the vapor pressure of the ESEM sample chamber was raised to 1050 Pa, the water droplet started to bridge with droplets on the adjacent line. Since the micropatterning surface can confine liquid in distinct micropatterned